NREL/TP-451-4938 • UC Category: 271 • DE92010588

Microscopic Origins of Metastable Effects in a-Si:H and Deep Defect Characterization in a-Si,Ge:H Alloys

Annual Subcontract Report
1 February 1991 - 31 January 1992

NREL/TP--451-4938

DE92 010588

J. D. Cohen
University of Oregon
Eugene, Oregon

NREL technical monitor: B. von Roedern

National Renewable Energy Laboratory
1617 Cole Boulevard
Golden, Colorado 80401-3393
A Division of Midwest Research Institute
Operated for the U.S. Department of Energy
under Contract No. DE-AC02-83CH10093

Prepared under Subcontract No. XG-1-10063-1

July 1992

On September 16, 1991 the Solar Energy Institute was designated a national laboratory, and its name was changed to the National Renewable Energy Laboratory.

Printed in the United States of America
Available from:
National Technical Information Service
U.S. Department of Commerce
5285 Port Royal Road
Springfield, VA 22161

Price: Microfiche A01
Printed Copy A03

Codes are used for pricing all publications. The code is determined by the number of pages in the publication. Information pertaining to the pricing codes can be found in the current issue of the following publications which are generally available in most libraries: *Energy Research Abstracts (ERA)*; *Government Reports Announcements* and Index (*GRA* and I); *Scientific and Technical Abstract Reports (STAR)*; and publication NTIS-PR-360 available from NTIS at the above address.

DISCLAIMER

Portions of this document may be illegible electronic image products. Images are produced from the best available original document.

TABLE OF CONTENTS

LIST OF ILLUSTRATIONS

Page

LIST OF TABLES

EXECUTIVE SUMMARY

During this first Subcontract year, our efforts have been primarily focussed on using transient photocapacitance and photocurrent measurements to determine the deep defect distribution and processes in low bandgap a-Si,Ge:H alloys. Samples for these studies were produced by the photo-CVD growth method and obtained through a collaboration with researchers at the University of Delaware. We discuss how a detailed comparison between the photocapacitance and photocurrent spectra can be used to examine separately the majority and minority carrier processes. Thus, we are not only able to map out the defect distributions in these samples, but also to determine an effective $\mu\tau$ product for the minority carriers. Specifically, the results of our studies indicate that: (1) the midgap defect densities in the alloy regime near 1.3 eV can be as low as 5×10^{16} cm^{-3} in such photo-CVD samples; (2) there exists a second defect band roughly 0.4 eV below E_C of a similar magnitude to the midgap defect density which exhibits significant lattice relaxation behavior in its electron trapping dynamics; (3) the hole $\mu\tau$ products determined for the lowest defect sample is roughly 5×10^{-10} cm^2/V, comparable with the highest hole $\mu\tau$'s reported in sandwich geometry measurements for alloys in this composition range; and (4) the hole mt is found to be roughly inversely proportional to the midgap defect density for the samples studied. This is consistent with the fact that the effective minority carrier lifetime for such measurements is limited by the deep state trapping time.

1.0 INTRODUCTION

The work carried out in our first subcontract year under NREL Subcontract XG-1-10063-1 has been mainly concentrated on the evaluation of the defect structure in a-Si,Ge:H materials in the relatively low bandgap alloy regime. The development of these low bandgap alloys with improved opto-electronic properties is essential for attaining the greatly improved efficiencies inherently possible in tandem cell structures. Most of what is actually known about the defect structure in such alloys has been obtained from survey studies utilizing ESR [1,2] methods which have indicated the presence of at least two kinds of intrinsic deep defects in the a-Si,Ge:H alloys with distinct g-factors, associated with dangling bonds on Si and Ge atoms. However, estimates of the energy positions of these defects within the gap currently have varied somewhat among different research groups.

We believed that the application of our capacitance based deep defect spectroscopic methods would greatly improve the understanding of the defect structure of these materials. One problem has been that, as the Ge fraction is increased much beyond about 30%, the overall quality of these alloys is found to degrade significantly. It then becomes difficult to obtain samples with significantly good barriers for capacitance measurements. However, based upon recent evidence from several laboratories that a-Si,Ge:H samples with fairly low defect densities could now be produced, we proposed utilizing such methods. Indeed, our first year's work under this Subcontract attests to the success of this approach.

We obtained several a-Si,Ge:H samples produced by the photo-CVD method in collaboration with Dr. Charles Fortmann at the IEC (with optical gap of 1.35 eV or less). We were then able to carry out an investigation of the defect structure in the a-Si,Ge:H alloy system using drive-level capacitance profiling, photocapacitance spectroscopy, and transient photocurrent spectroscopy. This resulted in allowing us to develop a fairly detailed picture of the deep defect distribution in a-Si,Ge:H materials in this alloy range.

In the Sections that follow, we first describe our basic methods and then discuss our detailed results on several a-Si,Ge:H samples as well as one a-Ge:H sample. We will also discuss the advantages of our sub-band-gap optical methods over more traditional methods. In particular, we will demonstrate how a comparison between the photocapacitance and transient photocurrent spectra can be used not only to disclose the features in the deep defect distribution within the gap, but also to learn about minority carrier processes such as the hole $\mu\tau$ products.

2.0 EXPERIMENTAL METHODS

The general method of junction transient measurements on amorphous semiconductors has been discussed in detail in several earlier publications.[3,4,5] The basic physics of all such measurements is as shown in Fig. 1. We illustrate the situation for a semiconductor with one discrete deep gap states within the space charge region of a Schottky barrier which is subjected to a voltage "filling pulse". This pulse causes a non-equilibrium (filled) occupation of gap state to be established. As time progresses, the initial steady-state population is recovered through the excitation of trapped electrons to the conduction band where they can then move out of the depletion region under the influence of the electric field. In the dark this process proceeds entirely by the thermal excitation of trapped carriers. However, this process can be enhanced through optical excitation which is the basis of the photocapacitance and junction photocurrent techniques.

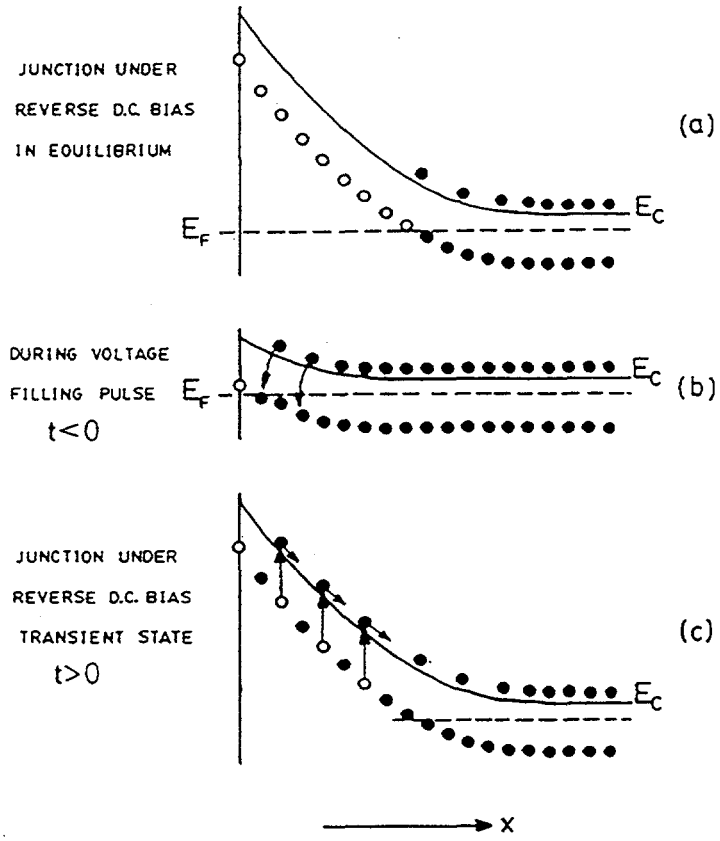

FIG. 1. Schematic diagram indicating the basic sequence of events in semiconducting junction transient measurements: (a) Junction under reverse bias in quasi-equilibrium showing the electronic occupation of gap states (solid circles) plus empty gap states above E_F in deep depletion (open circles). (b) During voltage "filling pulse" gap states capture electrons from the conduction band. (c) Reverse bias is restored and occupied gap states above E_F are slowly released to the conduction band due to thermal or optical excitation processes.

The re-equilibration can be observed by the redistribution of trapped carriers, either as a change in the *junction capacitance* (which occurs because the depletion region will contract as negative charge is lost and the positive charge density increases) or by monitoring the *current* which results from the motion of this charge. However, the observation of capacitance transients has one significant difference compared to current transient measurements: The dominant type of emitted carrier (electron or hole) can be identified by the *sign* of the observed change in capacitance. This implies that the direct comparison of capacitance and current transient measurements provides the means to explicitly separate the electron and hole emission and/or transport processes.

Instead of recording and analyzing the entire transient signal waveform, we process each transient in a manner to provide a single quantity that indicates the changes that occur over a specific timescale. This is accomplished by multiplying the transient signal, F(t), by a correlator A(t) that is a function of time, and then integrating over the time regime where the correlator is non-zero. This algorithm was developed in the analysis of transient data for the DLTS measurement technique [3] and the quantity, S, that results is therefore usually called the "DLTS signal" for a particular "time window", τ:

$$S(T,\tau,\omega) = \int_{t_1}^{t_2} A(t)\, F(t,T,\omega)\, dt \qquad (1)$$

Here we have indicated that all signals will depend on the temperature, T, and that capacitance signals will also depend on the measurement (angular) frequency, ω. The shape of the correlator function A(t), together with the limits of integration t_1 and t_2, determine the value of the effective time window parameter τ.

In the traditional DLTS method one fixes τ and records $S(T,\tau,\omega)$ in the dark as a function of temperature. The transient in this case is due primarily to the *thermal* excitation of trapped electrons (or holes) out of gap states. The measurement temperature determines the thermal energy depth, E_e, at which the trapped carriers can be emitted at the chosen time window:

$$E_e(T,\tau) = k_B T \log(\nu\tau) \qquad (2)$$

where ν is thermal emission rate prefactor and typically lies in the range 10^{12} to 10^{13} s^{-1}.[3]

In our photocapacitance (or photocurrent) measurements we fix both τ *and* the temperature and record such transients alternately in the dark and in the presence of

sub-band-gap light. The experimental details to accomplish this have been discussed previously.[6,7,8] We then define the photocapacitance (or photocurrent) signal, $P(E_{opt})$, to be the photon flux (Φ) normalized difference in the DLTS signals recorded with and without the presence of the sub-band-gap light of optical energy E_{opt}:

$$P(E_{opt},T) = \frac{S_{light}(T,\tau,\omega) - S_{dark}(T,\tau,\omega)}{\Phi(E_{opt})} \qquad (3)$$

Because both S_{light} and S_{dark} contain the same contribution of *thermally* emitted charge, P discloses the purely optically excited component of the release of gap state carriers.

The photocapacitance *spectrum* is obtained by plotting P *vs.* E_{opt} at constant T. We take special care to always operate in the low light intensity limit (where P is intensity independent). Thus the photocapacitance spectrum reveals the distribution of allowable transitions for an electronic population of gap states not appreciably disturbed by the optical excitation, but rather determined by the application of the voltage pulse followed by whatever thermal evolution takes place within the time before the transient is recorded.

Several examples of photocapacitance spectra are given in the following sections and have the general appearance of spectra obtained by the perhaps more familiar steady-state sub-band-gap optical techniques, such as photo-thermal deflection spectroscopy (PDS) [9] or the constant photocurrent method (CPM). [10] Indeed, one encounters a rather similar expression in the interpretation of our transient photo-spectra in terms of a convolution between localized gap states and extended states connected by an optical matrix element for the transitions. Specifically, for transitions from gap state electrons to the conduction band one expects a contribution to P given by [8,9]:

$$P_n^C(E_{opt},T) = K_n(T) \int_{E_c-E_{opt}}^{E_c-E_e} |\langle i|ex|f\rangle|^2 \, g(E) g_c(E+E_{opt}) dE \qquad (4)$$

where $|\langle i|ex|f\rangle|^2$ represents the optical matrix element, and $K_n(T)$ is a constant that depends on the temperature as well as the overall depletion width and the time window parameter τ (and also the frequency for the case of capacitance measurements). It will also depend on the ability of the carriers, once optically excited into the conduction band, to leave the depletion region. Thus K will depend on the electric field distribution within the depletion region and the electron mobility. However, all of

these factors will be roughly constant (independent of optical energy) for a given temperature and applied bias. One should also note that the upper limit of the integral is determined by the thermal escape depth, E_e, of gap state electrons to the conduction band at the measurement temperature and time window as given by Eq. (2). That is, the optical transitions from these shallower electronic levels will be missing from the photocapacitance spectrum because they will have escaped thermally before the photocapacitance signal is recorded.

We should stress that the expression given in Eq. (4) represents only one contribution to the photocapacitance or photocurrent signals. A similar expression [giving a quantity we might label $P_p^V(E_{opt})$] must be included to take into account transitions from the valence band into empty gap states. The leading constant will then be replaced by $K_p(T)$ which contains information about how easily the optically excited holes will leave the depletion region.

There are actually two other sub-band-gap optical processes that must be considered as well. First of all, an electron from the valence band can be excited into an empty gap state that is close enough to E_C that it will subsequently thermalize into the conduction band. This will occur on the timescale of our measurement if it lies within an energy E_e of conduction band mobility edge, and can be represented by the integral

$$P_n^V(E_{opt},T) = K_n(T) \int_{E_c-E_e}^{E_c} |\langle i|ex|f\rangle|^2 \, g(E) g_V(E-E_{opt}) dE \qquad (5)$$

With such a process there is also a hole left in the valence band. However, this has already been included in the expression for P_p^V. And, there will be an analogous integral expression for P_p^C resulting from optical transitions from deep in the mobility gap to the conduction band such that the hole that is left in the gap will thermalize the valence band on the measurement timescale.

A schematic diagram indicating these four types of processes in given in Fig. 2. Without additional information it is obvious that a single type of sub-band-gap spectrum will not allow one to distinguish the above possible contributions responsible for the observed signals. For example, PDS measurements are totally insensitive to the subsequent motion of carriers and therefore have absolutely no way to distinguish between such different types of transitions. Proponents of the CPM method argue that at low temperatures one can generally neglect the contribution of minority carrier

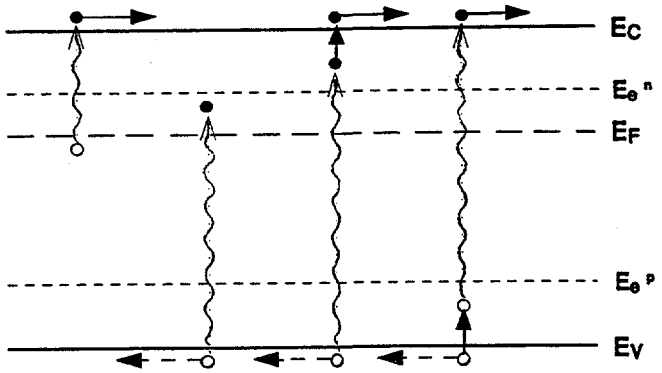

FIG. 2. Schematic diagram of the types of optically initiated deep defect transitions. As discussed in the text, these contribute differently to the photocapacitance and the transient photocurrent signals. Here optical transitions are indicated by wavy lines and thermal transitions are indicated by solid vertical lines. Horizontal arrows indicate electron and hole transport out of the depletion region. The dashed horizontal lines for the hole motion illustrate the fact that holes are more likely to be re-trapped before escaping the depletion region.

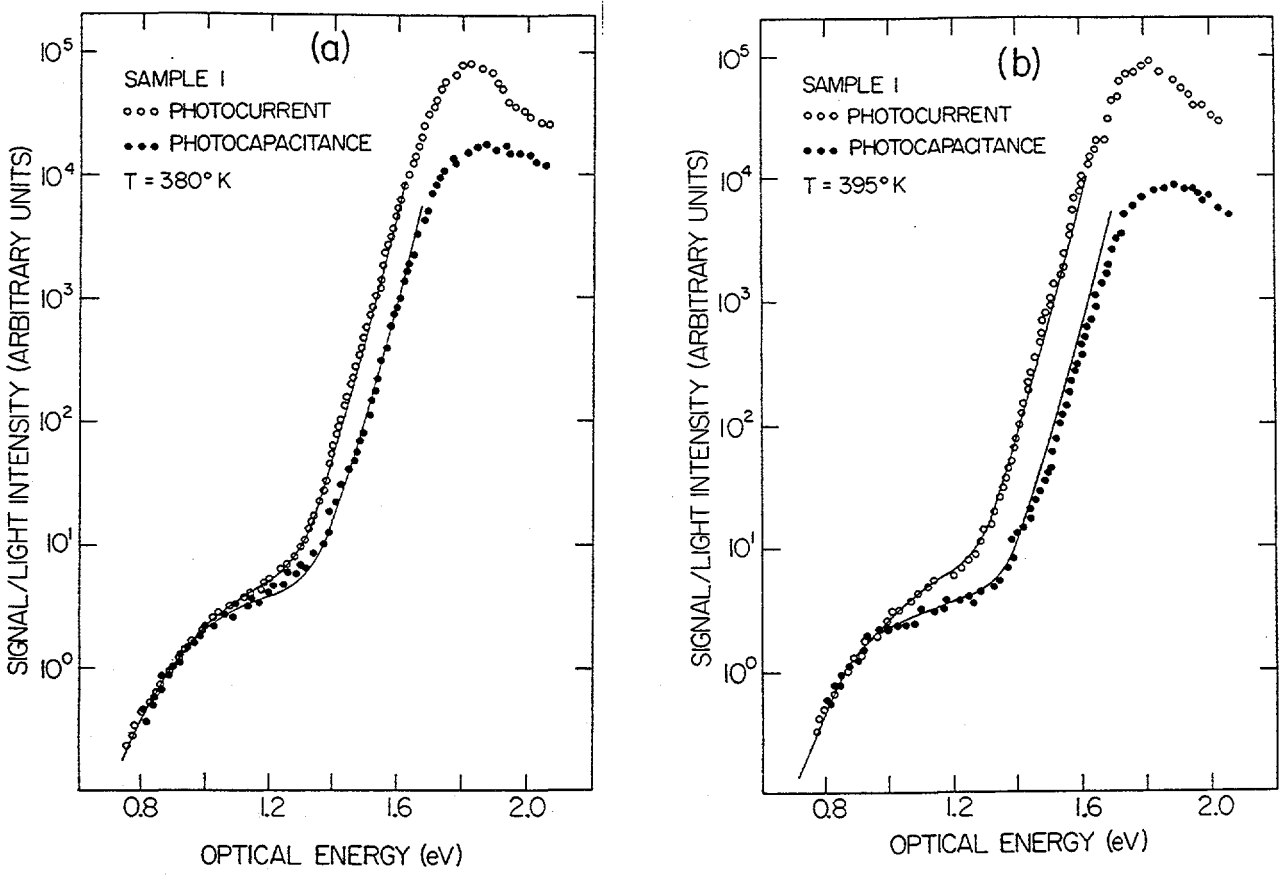

FIG. 3. Comparison of transient photocapacitance (solid circles) and transient junction photocurrent spectra (open circles) for an intrinsic a-Si:H sample at two temperatures: (a) 380K; and (b) 395K. The two types of spectra have been overlapped in the low optical energy regime for each temperature. The thin solid lines are the results of model calculations based on the set of defect transitions shown in Fig. 2.

motion to the current signal. However, one still has no way to separate the contributions to the electron current from the first two processes indicated in Fig. 2. Indeed, the contribution of the second type of process in the analysis of CPM data has incorrectly been completely neglected in the analysis of such spectra that have appeared in the literature.

Our studies, which compare the photocapacitance and photocurrent spectra resulting from the same set of electronic transitions, provide one of the few methods to identify the different types of transitions in Fig. 2. That is, the resulting integral expressions for P_n^C, P_p^V, P_n^V, etc., contribute differently depending upon whether one is considering a photocapacitance as opposed to a photocurrent spectrum. Thus, the two spectra taken together provide the information necessary to separate these.

To illustrate this procedure we can review our previous results obtained in this manner several years ago for a-Si:H. In Fig. 3 we show two pairs of spectra -- transient photocapacitance and transient photocurrent at two different temperatures -- for a low defect, intrinsic a-Si:H sample. We have aligned the two kinds of spectra on the vertical scale so that they overlap in the energy regime below 0.9 eV at each measurement temperature. As we have discussed previously [8,11], this is the regime where both kinds of measurements should respond to gap state transitions in the same manner since, for optical energies less than $E_g/2$, no optically excited hole transitions can occur (see Fig. 2). That is, if the only transition possible is the excitation of trapped gap state electrons to the conduction band, we will have purely an electron current. We thus define the relative magnitudes of our two kinds of signals to have a 1-to-1 ratio under these conditions.

At excitation energies larger than $E_g/2$, however, the other types of transitions indicated in Fig. 2 become possible. In the transient photocurrent measurements the motion of charge of either sign gives currents of the same sign so that the contributions will be *additive*. In contrast, in a photocapacitance measurement such processes will correspond to opposite changes in depletion charge and thus be *subtractive*. The relative weighting factors will depend on the field distribution throughout the depletion region and also the ability of the emitted hole to leave the depletion region.

The electron or hole which remains in a gap state following optical excitation is more likely to be *thermally* emitted at higher temperatures where thermal emission processes are faster. In general, such effects tend to cancel the optically induced charge change within the depletion region so that the photocapacitance signal is reduced.

However, the photocurrent signal will always be enhanced by any further motion of the charge. Thus we observe in Fig. 3 that the difference between the two kinds of signals does indeed become larger as the temperature is increased.

We have established previously that if n_e electrons and n_h holes leave the depletion region, and if release of carriers is uniformly distributed over the space-charge region, then the total transient current signal will roughly be proportional to $n_e + (1/2)n_h$ while the total transient capacitance signal will be proportional to $n_e - n_h$. [12] The factor of 1/2 for hole processes in the current signal arises because of the different spatial sensitivity for majority and minority carrier emission of that process. The capacitance signal, on the other hand, will have a nearly identical spatial sensitivity for both types of emission.

In the bandtail region of the spectra ($E_{opt} \geq 1.4$ eV), the optical excitation should release electrons and holes in roughly equal numbers. Indeed, the ratios of the photocapacitance and the photocurrent are quite constant over the range: $1.4 \text{ eV} \leq E_{opt} \leq 1.7$ eV. If all of the photo-released charges escaped, however, we would expect that the photocapacitance signal would be nearly zero. Due to the relatively high mobility of electrons in a-Si:H plus the relatively large electric fields in the depletion region, it is quite likely that all the released electrons *do* escape. Therefore, because the photocapacitance is only *partially* suppressed relative to the photocurrent signal, a significant fraction of the emitted holes must become re-trapped within the depletion region. From the ratios of the photocurrent to the photocapacitance signals in the exponential bandtail region we can determine that only 67% of the trapped holes are swept out of the depletion region at 380K. This increases roughly to 84% at 395K. These escape fractions of the minority carrier from the depletion are directly related to the $\mu\tau$ products of the holes. The details of the analysis required to find $\mu\tau$ from the ratio of the photocapacitance and photocurrent in the bandtail region is discussed in Section 4.2.

In the energy regime below 1.4 eV, we observe that the difference between the photocapacitance and photocurrent signals decreases monotonically to zero. Assuming a reasonable distribution of deep defects over the midgap region plus a simple thermally activated carrier emission process, we were able to model the experimental spectra quite successfully over the range of experimental temperatures. [11] The results of this modeling are indicated by the thin solid lines in Fig. 3. The set of transitions incorporated into these calculations include all of those discussed previously, as shown schematically in Fig. 2.

3.0 SAMPLES

The a-$Si_{1-x}Ge_x$:H samples used in our studies over the past year were obtained through an on-going collaboration with Charles Fortmann of the Institute for Energy Conversion at the University of Delaware. The films were depositied on p^+ crystalline silicon substrates by the photo-CVD method in which mixtures of SiH_4 and GeH_4 gases diluted in H_2 (total chamber pressure of 5 torr) are decomposed by UV radiation from a Hg vapor light source. The substrate temperature during growth was 230°C. Further details of this technique are given elsewhere. [13] The 2 samples investigated in detail to date for this study were found to have Tauc gaps near 1.3 eV and are thus believed to contain a germanium composition fraction (x) of roughly 0.6.[14] These photo-CVD samples are found to exhibit high photoconductivities (3 to 5×10^{-6} Siemens/cm) that are comparable to the best such alloy samples grown by the glow discharge method. Indeed, we found these samples to be among the lowest defect density a-$Si_{1-x}Ge_x$:H alloy samples currently available.

We deposited a 0.5 mm diameter (2×10^{-3} cm^2) semitransparent top contact of Pd on all samples. Our samples thus consisted of a p^+ buried junction in series with the front metal Schottky barrier. The material in the vicinity of either barrier could be selected for study depending on the polarity of the applied bias; however, the results presented here will be given for an applied bias which probes the substrate junction. This junction was found to exhibit lower leakage currents for both the a-Si:H and a-Si,Ge:H samples.

One pure a-Ge:H produced by the photo-CVD method was also studied. However, in contrast to the a-Si,Ge:H sample, only a limited assessment of its electronic properties could be obtained due to the much higher defect levels in this sample. This precluded our being able to obtain reliable photocapacitance spectra for this sample.

4.0 EXPERIMENTAL RESULTS

4.1 RESULTS FOR AMORPHOUS SILICON-GERMANIUM ALLOYS

Two pairs of photocapacitance and photocurrent spectra are shown for one of our a-Si,Ge:H samples in Fig. 4. As discussed in Section 2, we have overlapped these spectra at low optical energies since this should correspond to a single carrier excitation regime. For temperatures of 300K and below, we observe that the two kinds of spectra are nearly identical. This indicates that any photo-generated free holes are re-trapped

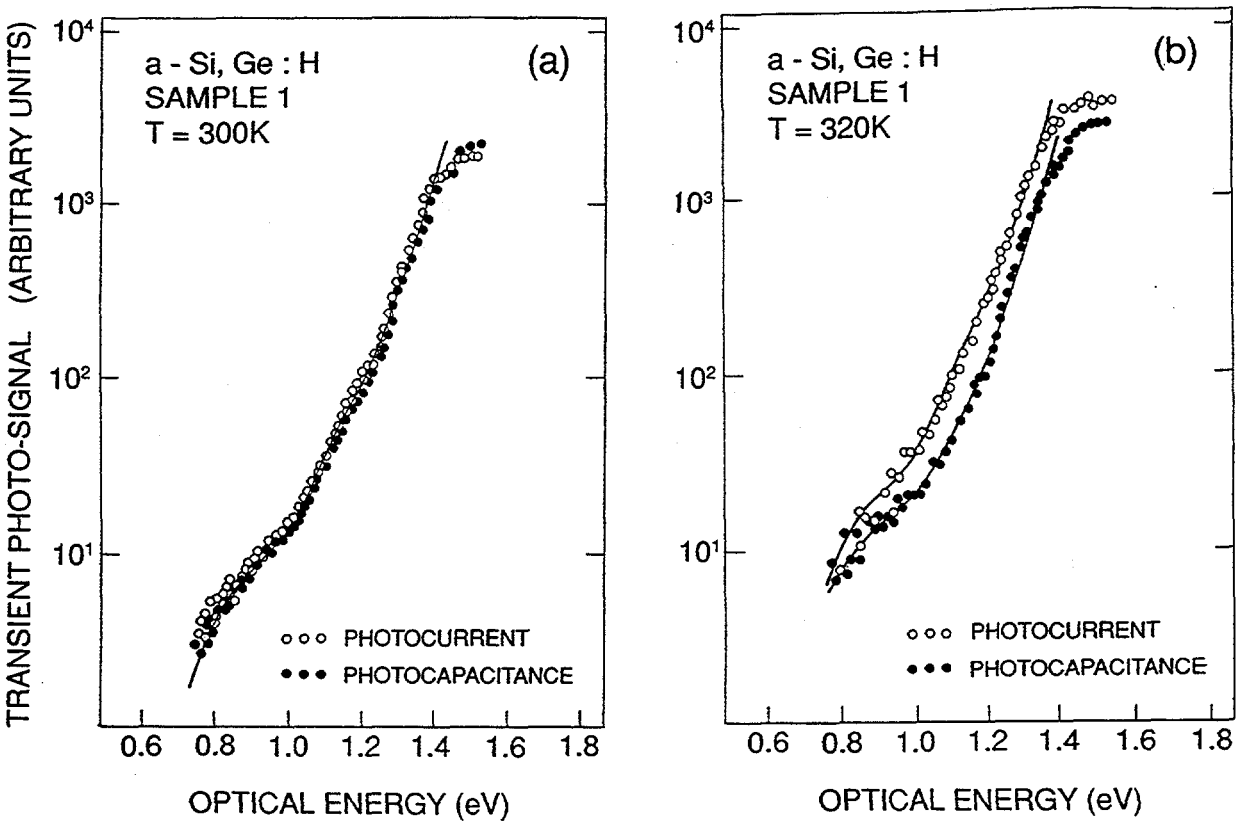

FIG. 4. Comparison of transient photocapacitance (solid circles) and transient junction photocurrent spectra (open circles) for an a-Si,Ge:H alloy sample at two temperatures: (a) 300K; and (b) 320K. The two types of spectra have again been overlapped in the low optical energy regime for each temperature. Solid lines are the results of model calculations based on the set of defect transitions shown in Fig. 5.

FIG. 5. Schematic of possible optical and thermal transitions for interpreting the a-Si,Ge:H spectra of Fig. 4. Different kinds of processes are depicted in the same as manner described in Fig. 3. The light dotted line for the thermal transition step in transition type 2' indicates that the electron emission from this process appears to be somewhat suppressed.

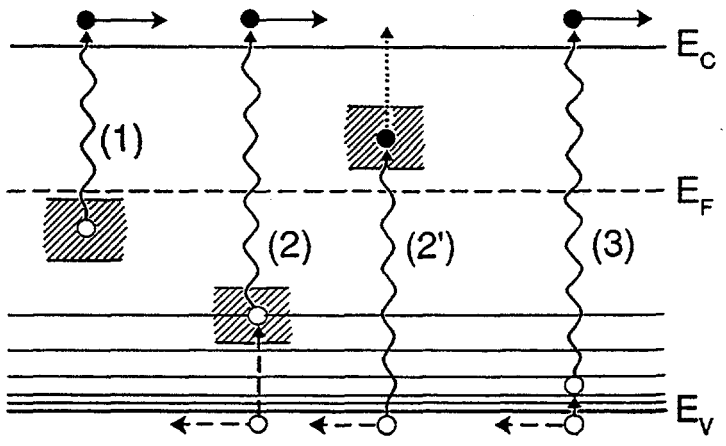

after a very short distance and that there is insufficient thermal energy to re-excite them into the valence band within the 0.4 second time window of the measurement. (A similar coalescing of the two kinds of spectra occurs for a-Si:H below 360K.) Although one cannot analyze such results at lower temperatures to obtain any information about minority carrier processes, the collapse of the two spectra into a single curve *does* provide an important test of the spatial uniformity of our sample because of the different spatial sensitivities of the capacitance and current signals.

Increasing the temperature to 320K produces the splitting of the two kinds of signals at larger optical energies indicative of the hole processes discussed above for a-Si:H. This difference was found to increase up to 330K and then to remain fairly constant. The ratio between the photocapacitance and photocurrent signals in the bandtail regime remains much closer to unity than for our previous a-Si:H studies. This indicates that mobilities are generally significantly lower in a-Si,Ge:H than in a-Si:H. This conclusion will be discussed in more detail in the next section.

A second major difference with a-Si:H is also observed. That is, while the ratio of signals for $E_{opt} \geq 1.2$ eV is fairly constant, the difference actually *increases* for lower energies (1.13 eV $\leq$ Eopt $\leq$ 1.22) before finally decreasing to zero in the lowest energy regime. This same behavior has been observed for several other a-Si,Ge:H samples in this alloy range. It is interesting to note that this intermediate energy regime (where the difference signal is the largest) also stands out in the lower temperature spectra as a region with a distinctly different slope.

We have again included a schematic (Fig. 5) of the possible types of transitions that we expect to be able to optically excite at different optical energies. At the lowest energies we again expect only a single type of carrier excitation (transition type 1). At intermediate energies we expect to be able to excite both trapped electrons out of the gap into the conduction band (transition type 2) and valence band electrons into the gap (transition type 2'). However, unlike a-Si:H where the relative importance of hole processes increases monotonically with increasing optical energy, there appears to be a maximum in the relative contribution of the hole process near an energy of 1.15 eV. This suggests a deep defect with somewhat unusual properties lying in the upper half of the mobility gap.

Finally, at energies approaching and/or exceeding the mobility gap, electrons and holes will be excited in equal numbers so that the relative magnitudes of the current and capacitance signals will depend only on the details of majority and

minority carrier transport. This regime is apparently reached for optical energies exceeding 1.2 eV in this sample.

A similar set of spectra are shown in Fig. 6 for a second a-Si,Ge:H sample. This sample had the same nominal germanium fraction as for sample 1, although our measurements indicated a slightly higher optical gap (1.35 *vs.* 1.28 eV). The *qualitative* behavior of this sample are very similar to sample 1, including the anomalous increased splitting between the photocapacitance and photocurrent spectra in the intermediate energy regime at higher temperatures. *Quantitatively*, however, the properties of this second sample appear markedly superior. In Fig. 6 we observe a somewhat narrower bandtail (52 meV *vs.* 57 meV) and evidence for lower defect density (from the relative positions of the top of defect band of transitions near 1.1 eV to the magnitude of signal near the optical gap energy). The drive-level profiling measurements [15] also indicated that this sample exhibited a low defect density near midgap of roughly 5×10^{16} cm^{-3} *vs.* about 3×10^{17} cm^{-3} for sample 1. This sample thus appears to exhibit defect properties as good or superior to any such low gap a-Si,Ge:H alloys yet reported.

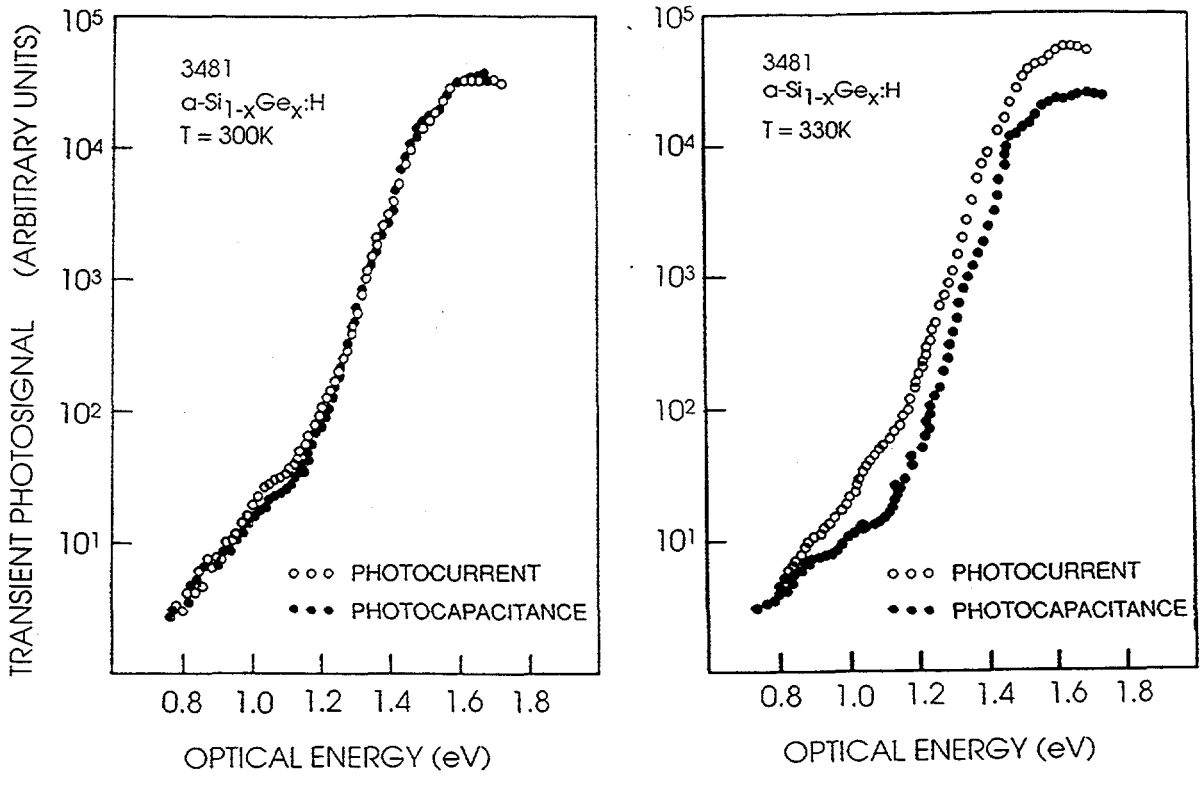

FIG. 6. Comparison of transient photocapacitance (solid circles) and transient junction photocurrent spectra (open circles) for a second a-Si,Ge:H alloy sample at two temperatures: (a) 300K; and (b) 330K. The two types of spectra have again been overlapped in the low optical energy regime for each temperature.

4.2 DETERMINATION OF CARRIER MOBILITIES

We have discussed that the ratio of the photocapacitance and photocurrent signals in the bandtail region of these spectra indicates the relative escape fractions of electrons and holes. We now will discuss how this information is directly related to the effective $\mu\tau$ product for the minority carrier motion.

Whether a carrier is optically created or occurs as a result of thermal emission, there is a significant probability that it will be re-trapped in a deep state before it leaves the depletion region. Because of the large electric fields within the depletion region and the generally larger electron mobilities compared to hole mobilities, this is probably only an issue for the *hole* transport and we will consider in detail only hole re-trapping. However, at the end of this Section we will discuss to what degree a small electron mobility might alter our conclusions.

We define $L_h(x)$ to be the average distance that a hole will travel after it is introduced into the valence band at a distance x from the barrier interface. The quantity L_h depends on x because the electric field, ε, varies considerably with position inside the depletion region. We may express the re-trapping lifetime for such holes, τ_h, by the expression

$$\tau_h(x) = \int_x^{x-L_h(x)} \frac{dx'}{v_h(x')} \qquad (6)$$

where the hole velocity, $v_h(x')$, is given by the product of the hole mobility, μ_h, and $\varepsilon(x')$. Since the hole re-trapping processes should be reasonably independent of the electric field, τ_h should be independent of the position x. In that case, given the electric field distribution (which can be obtained by solving Poisson's equation for a particular defect charge distribution), we may use Eq. (6) to obtain $L_h(x)$ in terms $(\mu\tau)_h$.

An analytic but approximate solution can be obtained by assuming the charge density is nearly constant throughout the depletion region. This approximation is quite accurate in deep depletion and, we have found, leads to a value of $(\mu\tau)_h$ that is almost always within a factor of 1.2 of a full numerical solution. In this "abrupt depletion" approximation, there exists a well defined depletion width, W, plus an electric field that varies linearly with the distance x from the barrier interface:

$$\varepsilon(x) = -\frac{q_e N_+}{\varepsilon} (W-x) \qquad (7)$$

Here q_e is the electronic charge, N_+ is the (assumed constant) charge density in deep depletion, and ε is the dielectric constant. An appropriate value of N_+ is determined experimentally from C-V methods [16].

We discussed in Section 2 above that if n_e electrons and n_h holes leave the depletion region during the measurement time window that the ratio R of the photocapacitance to junction photocurrent is approximately:

$$R = \frac{n_e - n_h}{n_e + n_h/2} \qquad (8)$$

The value of R is thus obtained directly from our experimental spectra and, in the abrupt depletion approximation, is found to be simply related to the $\mu\tau$ product for holes. Specifically one obtains:

$$(\mu\tau)_h = \frac{\varepsilon}{q_e N_+} \log [(R + 2)/3R] \qquad (9)$$

The details of this derivation have been presented elsewhere. [17] For a-Si:H, using the data in the bandtail region displayed in Fig. 3, we have R = 0.11 at 395K. From drive-level profiling measurements on this sample we have determined $N_+ \cong 2.0 \times 10^{15}$ cm^{-3} in deep depletion. Thus we obtain a $(\mu\tau)_h$ value of 6.0×10^{-9} cm^2/V.

To compare this value with those of other methods we note that our method determines $(\mu\tau)_h$ in a sandwich sample geometry at very low light intensities in a manner that is based on determining the escape distance of the minority carrier from the depletion region. Thus, this result should be generally consistent with those obtained with time-of-flight techniques rather than steady-state photoconductivity methods. That is, our effective lifetime depends on minority carrier deep-trapping rather than recombination, as discussed recently in detail by Crandall and Balberg. [18] We do indeed find our values to be in quite good agreement with the hole $\mu\tau$ products determined by time-of-flight measurements for high quality a-Si:H samples. [19,20]

If we again assume a much higher electron mobility than hole mobility for a-Si,Ge:H we may apply Eq. (9) without modification. From C-V data for sample 1 we estimate that $N_+ \cong 1.0 \times 10^{17}$ cm^{-3} in deep depletion. [16] For the 320K data in the bandtail regime the ratio R of photocapacitance to photocurrent is 0.5. Thus we obtain $(\mu\tau)_h = 3.3 \times 10^{-11}$ cm^2/V; that is, a value roughly 200 times smaller than in a-Si:H.

Sample 2 which exhibited a much narrower bandtail slope (52 meV compared to about 58 meV for sample 1), also exhibited a much lower deep depletion charge density ($N_+ = 2 \times 10^{16}$ cm^{-3}), and a smaller R ratio (0.3 at 330K). We thus obtain a value of $(\mu\tau)_h$ for this sample of 5×10^{-10} cm^2/V. This value is in quite good agreement with the best values reported for undoped samples in this alloy regime by the analysis of the internal quantum efficiency *vs.* reverse bias on Schottky diode devices.[20] We note, however, that the analysis of those measurements employs some simplifying assumptions which, we believe, will tend to overestimate the value of $(\mu\tau)_h$. Hence we believe that our sample 2 may actually exhibits superior properties to those previously reported for this composition range.[21]

There has been some evidence that a-Si,Ge:H alloys exhibit quite poor electron mobilities, perhaps as low as for its hole mobility deduced above. [22] We should therefore discuss somewhat further our assumption that all emitted electrons are able to escape the depletion region.

For the a-Si,Ge:H data presented in this report, a more detailed analysis shows that as long as $(\mu\tau)_e$ is greater than about ten times $(\mu\tau)_h$, the values of $(\mu\tau)_h$ will not be appreciably modified. Even if $(\mu\tau)_e$ is within a factor of three, the deduced values of $(\mu\tau)_h$ will be reduced only by about 30%. Our deduced values will be appreciably modified only if $(\mu\tau)_e$ becomes less than or equal $(\mu\tau)_h$. However, our data can be used to absolutely rule out the possibility of $(\mu\tau)_e < (\mu\tau)_h$ (since then the photocapacitance signal in the bandtail region actually changes sign). On the other hand, they could be consistent with a value of $(\mu\tau)_h$ that agrees reasonably well with other measurements and yet allows a value of $(\mu\tau)_e$ that is within a factor of 2 to 3 times greater.

If $(\mu\tau)_e$ is indeed this low then we may be able to determine $(\mu\tau)_e$ directly from the ratio of the photocurrent to photocapacitance signals in the low optical energy limit. Unfortunately, the signal quality for $E_{opt} < 0.8$ eV does not permit this at the present time. However, we hope to pursue this further with better samples in the near future.

4.3 DETERMINATION OF DEEP DEFECT PROPERTIES

The spectra for a-Si,Ge:H in the defect band region exhibit some qualitative differences from the corresponding spectra of a-Si:H. At 300K [Fig. 4(a) and 6(a)] we observe indications of two distinct regions of sub-band-gap transitions: one extending from $E_g/2$ to about 1.0 eV, and the other form about 1.03 eV to 1.23 eV in optical energies. The most natural explanation for this is in terms of the two kinds of defect

transitions indicated schematically in Fig. 5. This implies that the lower energy regime corresponds to optical transitions into the conduction band out of a defect band lying below E_F (labeled as type 1), while the higher energy region originates from contributions of transitions of types 2 and 2'. A deep defect density has again been estimated by comparing these optical spectra with C-V data and indicates a defect density of about 2 to 3×10^{17} cm^{-3} in a broad band located roughly mid-gap. A more pronounced narrow defect band appears to be located roughly 1.1 eV above E_V of magnitude 4×10^{17} cm^{-3} with a FWHM of about 0.2 eV. The fit to the lower temperature data obtained for this deep defect structure is indicated for sample 1 by the solid line in Fig. 4(a).

Increasing the measurement temperature to 320K, one again observes a significant contribution from hole processes from the deviation of the two types of spectra. Unlike the a-Si:H case, however, we observe an *increase* of the ratio of photocurrent to photocapacitance for sample 1 from 2.0 in the bandtail region to about 2.6 at 1.15 eV. This behavior is qualitatively similar for sample 2. Only for optical energies decreasing below 1.1 eV does this ratio appear to decrease monotonically to unity.

The free carrier mobilities cannot depend on the details of how electrons and holes are introduced into the bands. Thus the relative increase of the photocurrent signal cannot be a result of changes in carrier mobility; rather, it indicates that the number of electrons arriving into the conduction band is itself relatively smaller in this energy regime. This seems to imply that the thermalization of electrons into the conduction band following their optical excitation from the valence band into empty gap states (transition type 2') is significantly suppressed. This would then tend to increase the hole current relative to the electron current in this optical energy regime. We have indicated this hypothesis on Fig. 5 by using a light dotted line to label the electron thermal emission step for transitions of type 2'. Assuming that the thermal release of electrons is suppressed is about 25% relative to holes gives the fits to the 320K data of sample 1 indicated in Fig. 4(b).

Such a significant suppression of the thermal emission rate of electrons at these temperatures following a 1.1 eV excitation above the valence band mobility edge forces us to conclude that there must be a significant degree of lattice relaxation for electrons occupying these deep states above midgap. This finding is quite consistent with very recent results of the Tauc group [12] in which photo-induced absorption studies of

a-Si,Ge:H alloys indicate that there exists a defect level above E_F which undergoes a lattice relaxation of about 0.4 eV.

4.4 AMORPHOUS GERMANIUM

We have attempted to carry out similar measurements on intrinsic a-Ge:H samples, but have so far been limited by the large defect density present in those samples. In particular, the small photo-response prohibited sufficient signal strength for the photocapacitance measurements in the low energy regime. Thus, we were not able to deduce ($\mu\tau$) products for our present samples.

The capacitance versus temperature measurements for our a-Ge:H samples show a much larger activation step than for a-Si:H and a-SiGe:H, which implies the presence of a large defect band close to the Fermi level. By fitting our data to the capacitance response of a density of states composed of a gaussian-shaped defect band below E_c we deduce a defect density of $N_d \cong 9 \times 10^{17} cm^{-3}$ located in a defect band at approximately 0.5eV below the conduction band edge E_c. We are thus tempted to associate this defect band with the feature we deduced in the a-Si,Ge:H alloys lying 0.4-0.5 eV below E_C. However, the optical spectra exhibit a threshold for a defect band that are reasonably consistent with the capacitance-temperature data. Hence, this seems to be inconsistent for a defect possessing a significant contribution due to lattice relaxation.

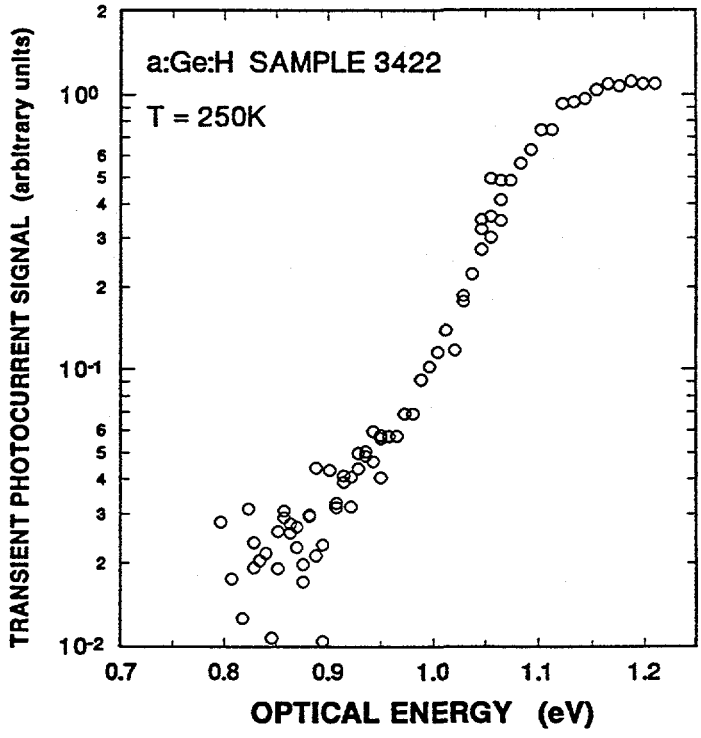

FIG. 7. Transient photo-current spectrum for an a-Ge:H sample recorded at 250K showing a quite narrow bandtail and also indicating a fairly large deep defect density (the region below about 1 eV). Unfortunately, the poor barrier properties of this sample did not permit a reliable photocapacitance spectrum to be obtained.

Another interesting observation is that despite the large defect density, we deduce an Urbach energy of 50meV which is comparable to values found for a-Si,Ge:H and a-Si:H samples with much lower defect densities. This tends to contradict models [23] that link the Urbach-tail energy to the density of deep defects.

5.0 SUMMARY AND CONCLUSIONS

In this presentation we have shown how a comparison between transient junction photocurrent and photocapacitance spectra can yield detailed information not only about the deep defect distributions and transition energies in amorphous semiconductors, but also about the carrier mobilities. This comes from the unique aspect of capacitance measurements to distinguish between minority and majority carrier processes.

A summary of the properties of the samples discussed in this report are presented in Table I. Previous results for the best a-Si:H studied by such experimental methods in our laboratory are included for comparison purposes. We observe that the minority carrier mobilities appear to scale roughly linearly with the midgap deep defect concentrations. This is consistent with a $(\mu\tau)_h$ limited by trapping processes into deep defect at or below E_F.

Our deduced $\mu\tau$ products for holes in a-Si,Ge:H were found to be in reasonably good agreement to those that have been obtained by other techniques on high quality

TABLE I. Summary of electronic properties of the a-Si,Ge:H and a-Ge:H samples presented in this report. The correponding properties of a high quality a-Si:H sample determined in the same manner are included.

SAMPLE	Optical Gap (eV)	Defect Density (cm^{-3})	Urbach Energy (meV)	Hole $\mu\tau$ (cm^2/V)
a-Ge:H	1.07	9×10^{17}	50	-----
a-Si,Ge:H	1.28	2.5×10^{17}	57	3×10^{-11}
a-Si,Ge:H	1.35	5×10^{16}	52	5×10^{-10}
a-Si:H	1.8	4×10^{15}	42	6×10^{-9}

material provided we make those comparisons to other methods that are trapping time rather than recombination time limited. Indeed, in this regard our values obtained on these photo-CVD alloy samples appear to be as good or superior to the best values quoted in the literature for this alloy range. One should note, however, that we obtained our values at relative higher temperature and possibly for higher values of electric fields than some of those other measurements. Finally, we discussed the suggestion that *electron* $\mu\tau$ products may be quite low in a-Si,Ge:H. While our data explicitly rule out a smaller $\mu\tau$ product for electrons than holes, we also find that our results would be consistent with an electron $\mu\tau$ perhaps only 2 or 3 times higher than that for holes in this material.

Regarding the types of defect transitions in a-Si,Ge:H, our results indicate that there exists a region of optical transitions (near $E_{opt} = 0.8$ eV) between a defect band 0.6 to 0.7 eV above E_V to the conduction band, and another band of transitions (near 1.1 eV) between the valence band and an empty defect sub-band above E_F. Our results also indicate that electronic transitions from this latter defect band to the conduction band are significantly suppressed. This behavior implies a significant degree of lattice relaxation for transitions from this defect, a conclusion which agrees with findings on a-Si,Ge:H obtained recently by the Tauc group using time resolved optically induced absorption measurements.

6.0 PERSONNEL

J. David Cohen	Principal Investigator/Program Manager
Randall Rasmussen	Research Associate: February 1991 to September 1991
John Hautala	Research Associate: September 1991 to February 1992
Thomas Unold	Research Assistant

ACKNOWLEDGEMENTS

We wish to thank A.V. Gelatos and K.K. Mahavadi for considerable help in the early stages of interpreting the photocapacitance measurements in intrinsic a-Si:H, and thank Charles Fortmann and Wayne Buchanen for the a-Si,Ge:H sample preparation.

REFERENCES

1. M. Stutzmann, C.C. Tsai, and R.A. Street, J. Non-Cryst. Solids 97&98, 1011 (1987).

2. F. Finger and W. Fuhs, Mat. Res. Soc. Symp. Proc. 118, 635 (1988).

3. Lang, D.V. in Thermally Stimulated Relaxation in Solids, vol. 37 of Topics in Applied Physics, ed by P. Braunlich (Springer, Berlin, 1979), p. 93.

4. Lang, D.V., Cohen, J.D., and Harbison, J.P., Phys. Rev. B25, 5285 (1982).

5. Cohen, J.D., in Hydrogenated Amorphous Silicon, vol. 21C of Semiconductors and Semimetals, ed. by J. Pankove (Academic Press, New York, 1984), p. 9.

6. Gelatos, A.V., Cohen, J.D., and Harbison, J.P., in Optical Effects in Amorphous Silicon, ed. by P.C. Taylor and S.G. Bishop (AIP Conf. Proc. No. 120, New York, 1984), p. 16.

7. Gelatos, A.V., Cohen, J.D., and Harbison, J.P., Appl. Phys. Lett., 49, 722 (1986).

8. Cohen, J.D., and Gelatos, A.V., in Amorphous Silicon and Related Materials, ed. by H. Fritzsche (World Scientific, Singapore, 1989), p. 475.

9. Amer, N.M., and Jackson, W.B., in Hydrogenated Amorphous Silicon, vol. 21B of Semiconductors and Semimetals, ed. by J. Pankove (Academic Press, New York, 1984), p. 83.

10. Vanacek, M., Kocka, J., Stuchlik, J., Kozisek, Z., Stika, O., and Triska, A., Sol. Energy Mat. 8, 411 (1983).

11. Gelatos, A.V., Mahavadi, K.K., Cohen, J.D., and Harbison, J.P., Appl. Phys. Lett. 53, 403 (1988).

12. Cohen, J.D., and Lang, D.V., Phys. Rev. B25, 5321 (1982).

13. Albright, D.E., Saxena, N., Fortmann, C.M., Rocheleau, R.E., Russell, T.W.F., AIChE Journal 36, 1555 (1990).

14. Chen, L., Tauc, J., Lee, J.-K., and Schiff, E.A., Phys. Rev. B43, 11694 (1991).

15. C.E. Michelson, A.V. Gelatos, and J.D. Cohen, Appl. Phys. Lett. 47, 397 (1985).

16. We use the asymptotic value of the drive-level profiling charge density as the temperature is increased. This should approach the deep depletion charge density as a limiting case. For a description of this method see reference 15.

17. J.D. Cohen, T. Unold, A.V. Gelatos, and C.M. Fortmann, J. Non-Cryst. Solids, in press.

18. R.S. Crandall and I. Balberg, Appl. Phys. Lett. 58, 508 (1991).

19. See, for example, Yamaguchi, M., Takada, J., Hosokawa, Y., and Tawada, Y., J. Non-Cryst. Sol. 77&78, 447 (1985).

20. Aljishi, S., Smith, Z E., and Wagner, S., in Amorphous Silicon and Related Materials, ed. by H. Fritzsche (World Scientific, Singapore, 1989), p. 887.

21. The analysis in terms of the internal quantum efficiency assumed, for example, that the electric field was uniform across the entire device and equal to the applied voltage divided by the film thickness. This certainly is *not* true for a Schottky barrier device and, in fact, the average electric fields will generally be significantly *larger*. This will produce an overestimate of the value of $(\mu\tau)_h$ that scales with the *square* of the factor by which the magnitude of the electric field was underestimated.

22. Fortmann, C.M., Albright, D.E, Campbell, I.H., and Fauchet, P.M., Mat. Res. Soc. Symp. Proc. 164, 315 (1990).

23. For example see S. Aljishi, Z E. Smith and S. Wagner, in *Amorphous Silicon and Related Materials*, ed. by H. Fritzsche, (World Scientific, Singapore, 1989) p. 887.

Document Control Page	1. NREL Report No. NREL/TP-451-4938	2. NTIS Accession No. DE92010588	3. Recipient's Accession No.

4. Title and Subtitle

Microscopic Origins of Metastable Effects in a-Si:H and Deep Defect Characterization in a-Si,Ge:H Alloys

5. Publication Date

July 1992

6.

7. Author(s)

J. D. Cohen

8. Performing Organization Rept. No.

9. Performing Organization Name and Address

Dept. of Physics and Materials Science Institute
University of Oregon
Eugene, Oregon

10. Project/Task/Work Unit No.

PV231101

11. Contract (C) or Grant (G) No.

(C) XG-1-10063-1

(G)

12. Sponsoring Organization Name and Address

National Renewable Energy Laboratory
1617 Cole Blvd.
Golden, CO 80401-3393

13. Type of Report & Period Covered

Technical Report
1 February 1991 - 31 January 1992

14.

15. Supplementary Notes

NREL technical monitor: B. von Roedern

16. Abstract (Limit: 200 words)

This report describes works to use transient photocapacitance and photocurrent measurements to determine the deep defect distribution and processes in low-band-gap a-Si,Ge:H alloys. Samples for these studies were produced by the photochemical vapor deposition (photo-CVD) growth method and were obtained through a collaboration with researchers at the University of Delaware. This report discusses how a detailed comparison between the photocapacitance and photocurrent spectra can be used to separately examine the majority and minority carrier processes. The results are as follows: (1) The midgap defect densities in the alloy regime near 1.3 eV can be as low as 5×10^{16} cm^{-3} in such photo-CVD samples. (2) There exists a second defect band roughly 0.4 eV below E_C of a similar magnitude to the midgap defect density that exhibits significant lattice relaxation behavior in its electron trapping dynamics. (3) The hole $\mu\tau$ products determined for the lowest defect sample are roughly 5×10^{-10} cm^2/V, comparable with the highest hole $\mu\tau$ products reported in sandwich geometry measurements for alloys in this composition range. (4) The hole $\mu\tau$ is found to be roughly inversely proportional to the midgap defect density for the samples studied. This is consistent with the fact that the effective minority carrier lifetime for such measurements is limited by the deep state trapping time.

17. Document Analysis

a. Descriptors

amorphous silicon ; characterization ; photovoltaics ; solar cells ; defects

b. Identifiers/Open-Ended Terms

c. UC Categories

271

18. Availability Statement

National Technical Information Service
U.S. Department of Commerce
5285 Port Royal Road
Springfield, VA 22161

19. No. of Pages

28

20. Price

A03